

## Extremes of Dissolved Oxygen in the California Current System

J. XAVIER PROCHASKA,<sup>a,b,c,d</sup> DANIEL RUDNICK,<sup>e</sup>

<sup>a</sup> *Affiliate of the Department of Ocean Sciences, University of California, Santa Cruz, CA 95064, USA*

<sup>b</sup> *Visiting Faculty, Scripps Institution of Oceanography*

<sup>c</sup> *Department of Astronomy and Astrophysics, University of California, Santa Cruz, CA 95064, USA*

<sup>d</sup> *Simons Pivot Fellow*

<sup>e</sup> *Scripps Institution of Oceanography*

**ABSTRACT:** Dissolved oxygen (DO) is a non-conservative tracer of interactions at the air-sea interface, respiration and photosynthesis, and advection. In this manuscript, we study extremes in the degree of oxygen saturation (SO), the ratio of DO to the maximum concentration given the water's temperature, salinity, and depth with SO=1 critically saturated. We perform the analysis with the California Underwater Glider Network (CUGN), which operates gliders on four lines that extend from the California coast to several hundred kilometers offshore, profiling to 500 m depth every 3 km. Since ~2017, the gliders have been equipped with a Sea-Bird 63 optode sensor to measure the DO content. We find that parcels with SO > 1.1, hyperoxic extrema, occur primarily near-shore in the upper 50 m of the water column and during non-winter months. Along Line 90 which originates in San Diego, these hyperoxic events occur primarily in stratified waters with shallow mixed layers. We hypothesize that photosynthesis elevates DO in sub-surface water that can not rapidly ventilate with the surface. Along the three other lines, hyperoxic extrema occur almost exclusively at the surface and are correlated with elevated Chl – a fluorescence suggesting they are primarily driven by blooms of photosynthesis. We also examine hypoxic extrema, finding that parcels with SO < 0.9 and  $z < 50$  m occur most frequently along the northernmost line where upwelling has greatest impact.

### 1. Introduction

The dissolved oxygen (DO) concentration is a fundamental property of ocean water and an essential ingredient for life throughout the ocean food web. This includes the respiration of fish and mammals as well as the growth of crustaceans and single-cell organisms that lie close to the base of the food web. DO enters the ocean through two main processes: (i) ventilation of air at the air-sea interface and (ii) biological production during processes like photosynthesis. DO is removed either through respiration or if an increase in temperature leads to a super-saturated state with the excess eventually fluxed through the air-sea interface. In addition, mixing redistributes oxygen, e.g., so that a region that is locally super-saturated could become less saturated.

Given the importance of DO, it has been a focus of global analyses which assess interannual changes (Helm et al. 2011; Schmidtko et al. 2017). Best estimates for the global ocean indicate an  $\approx 2\%$  decline in DO since 1960 and at a rate of  $\approx 10^{20} \mu\text{mol kg}^{-1} \text{yr}^{-1}$  (Schmidtko et al. 2017). The primary causes are believed to be (1) rising sea temperature which lowers the maximum oxygen concentration (OC) of water and (2) reduced ventilation to depth owing to greater ocean stratification (Keeling and Garcia 2002). These processes and their impacts on DO have been studied in a suite of climate models which consistently predict a decline in DO (Bopp et al. 2013), but show large variations in the regional distribution of this signal.

Regional observations, therefore, may impact and inform future models and (potentially) improve their success at predicting future changes on a warming Earth.

At the regional level, one of the few sites with long-term monitoring of DO is coastal California. Since 1984, the CalCOFI experiment has obtained DO measurements following standard protocol quarterly at 66 standard stations on 6 lines running several hundred kilometers off coastal California. These data provided one of the first conclusive indications that the DO concentration is declining (Bograd et al. 2008), at least within select regions. The origins for the decline have been proposed to be the advection of water with depleted DO into the region and decreased vertical transport due to increased stratification near the surface.

Since 2017, the California Underwater Glider Network (CUGN) has been measuring DO along several lines off the California coast (three since 2017 and an additional two since 2019) with an approximately 50 times higher profiling frequency than CalCOFI. These data have yielded a robust estimate of the annual cycle in DO (Ren et al. 2004, submitted) which resolves seasonal trends associated with the dominant processes along the California coast (e.g. upwelling). Furthermore, the CUGN dataset is now sufficiently large (over 150,000 profiles across the four lines) to search for rare events, i.e. outliers of hypoxic and/or hyperoxic water.

In this manuscript, we focus primarily on hyperoxic events, specifically episodes with super-saturated DO in excess of 10% of the maximum oxygen concentration. Our principal motivation is to explore the physical conditions

---

*Corresponding author:* J. Xavier Prochaska, [jxp@ucsc.edu](mailto:jxp@ucsc.edu)

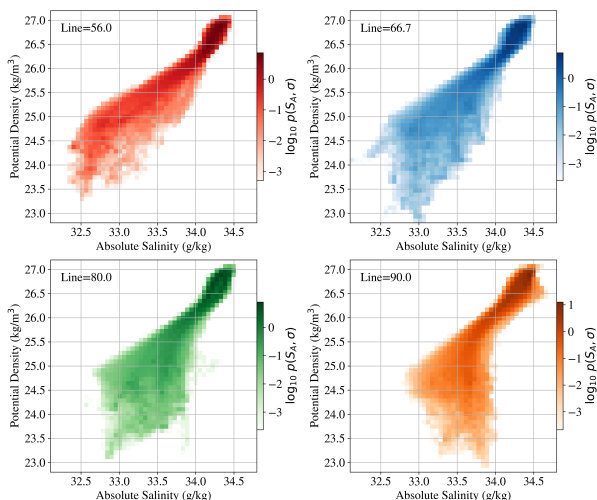


FIG. 1. Joint probability density functions  $p(S_A, \sigma_0)$  for the conserved quantities of potential density  $\sigma_0$  and absolute salinity  $S_A$  for all water cells along the four lines of the CUGN, restricted to those with a valid dissolved oxygen DO measurement. The bins have width  $\Delta S_A = 0.0551 \text{ g kg}^{-1}$  and  $\Delta \sigma_0 = 0.0898 \text{ kg m}^{-3}$  and start at  $(S_A, \sigma_0) = 32.1 \text{ g kg}^{-1}, 22.8 \text{ kg m}^{-3}$ . On all lines,  $p(S_A, \sigma_0)$  peaks on the high salinity, dense and cold water that occurs at depth ( $z > 200 \text{ m}$ ). The distribution then extends to lower  $\sigma_0$  and  $S_A$  where it exhibits a wider range of values. This broadening of  $p(S_A, \sigma_0)$  is due to several processes at the surface including the injection of fresh water, evaporation, and mixing. Note also the progression towards a higher incidence of lower  $\sigma_0$  (warmer) and higher  $S_A$  water as one trends southward from Line 56.0 to Line 90.0.

that drive any such phenomena. In turn, the results may offer insight into biological responses in the CUGN associated with rare (or common) physical events. Furthermore, extrema “stress test” models of complex systems which invariably include approximations of unknown or unresolved processes. As more advanced biogeochemical prescriptions are proposed for regional models (e.g. Fennel et al. 2006), constraints related to the incidence and generation of extrema will inform development and reliability. Last, hyperoxic waters have been touted as a pseudo-sanctuary for biological life in an otherwise warming ecosystem (Giomi et al. 2019).

## 2. Methods

### a. Data

The California Underwater Glider Network (CUGN) uses Spray gliders operated on five lines near central and southern coastal California. Four lines are directed offshore (named Lines 90.0, 80.0, 66.7, 56.0 following the CalCOFI convention) and a fifth is directed along shore (not analyzed here). The gliders are equipped with sensors to measure the in-situ temperature, salinity, fluorescence associated with chlorophyll, horizontal veloc-

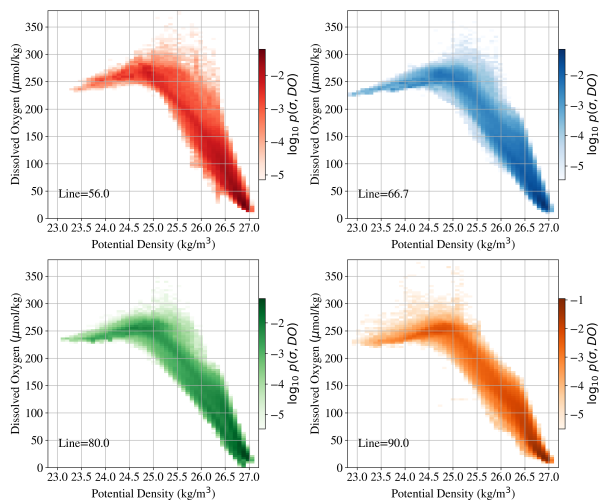


FIG. 2. Joint PDF for dissolved oxygen versus potential density  $p(\text{DO}, \sigma_0)$  for each of the four lines. The high density water, which occur at depth, exhibits the lowest DO, approaching  $0 \mu\text{mol kg}^{-1}$  at the greatest depths of the CUGN (500 m). One also notes that DO achieves a maximum on each line at intermediate  $\sigma_0$ . These occur are at or near the surface but in lower temperature water than that of the lowest density parcels. At these lower temperatures, the water can maintain a higher DO concentration.

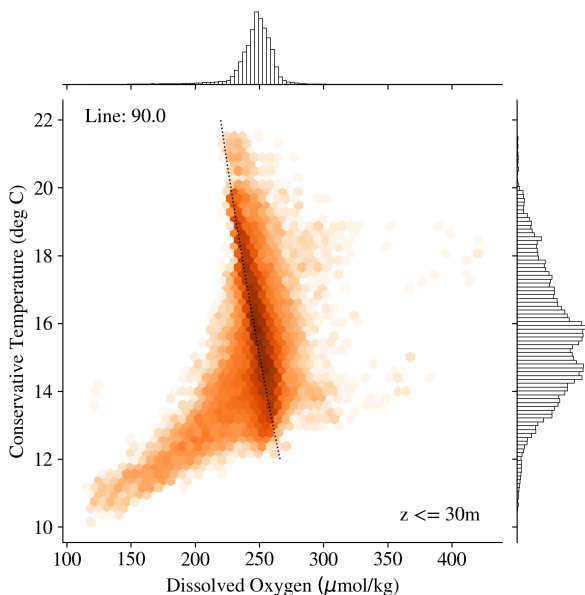


FIG. 3. Joint PDF  $p(\theta, \text{DO})$  of the conservative temperature  $\theta$  versus DO along Line 90.0 and restricted to depths  $z \leq 30 \text{ m}$ . The dotted black line indicates the maximum oxygen concentration (OC) for a fiducial absolute salinity ( $S_A = 33.7 \text{ g kg}^{-1}$ ). The majority of water parcels at these near-surface depths have an oxygen saturation  $\text{SO} = \text{DO}/\text{OC} \approx 1$ . However, the figure also reveals tails in DO to higher and lower values indicative of under and super-saturated waters, i.e. extrema that are the focus of this manuscript.

ity, and acoustic backscattering. Since 2017<sup>1</sup>, the Sprays have also included a Sea-Bird 63 optode sensor to measure the dissolved oxygen content, here reported in units of  $\mu\text{molkg}^{-1}$ . These sensors are regularly calibrated to achieve  $\approx 0.5\mu\text{molkg}^{-1}$  accuracy for DO measurements in the CUGN (Ren et al. 2023).

Each line is surveyed by a Spray glider (two on rare occasions) traveling up to 350-500 km offshore and back in a series of 500 m dives, one every  $\approx 3$  km. The sensors record measurements every 8 s or approximately 2 m horizontal distance and 1 m in the vertical. In this manuscript, we analyze the science quality, high-level data product gridded to cells of 10 m depth. Rudnick et al. (2017) provides a complete description of the optimal interpolation process used to construct the grid and an overview of the principle properties (e.g.  $T$ , velocity) measured along the first three lines of the CUGN including their annual cycles.

### b. Derived Quantities

For each gridded dataset for each line, we have calculated the conserved quantities of absolute salinity ( $S_A$ ), conservative temperature ( $\theta$ ) and potential density ( $\sigma_0$ ) following the Thermodynamic Equation Of Seawater - 2010 (TEOS-10) definitions (IOC, SCOR and IAPSO 2010), and adopting the grid depth and the average longitude and latitude of the line in the calculations. The joint probability density function PDF of absolute salinity and potential density  $p(S_A, \sigma_0)$  for each line is presented in Figure 1. The peak in  $p(S_A, \sigma_0)$  is at high salinity, high density water found at depth ( $z > 200$  m). As one heads to the surface, the distribution extends to lower  $\sigma_0$  and  $S_A$  and exhibits a wider range of values. The large range of  $\theta$  and  $S_A$  at the surface reflect interactions that modify temperature (e.g. solar heating, cooling) and/or salinity (e.g. evaporation, rainfall, river runoff). This study focuses on these surface waters. Examining the four panels together, one notes the progression towards a higher incidence of lower  $\sigma_0$  (warmer) and higher  $S_A$  water as one travels southward from Line 56.0 to Line 90.0. This reflects the greater influence of the California Undercurrent which advects warmer, saltier water from the equatorial Pacific Ocean into the CUGN (Rudnick et al. 2017).

Turning our attention to DO, Figure 2 shows the joint PDFs for DO against  $\sigma_0$ . The high density water, which occurs at depth, exhibits the lowest DO, approaching  $0\mu\text{molkg}^{-1}$  at the highest densities and depths of the CUGN ( $z = 500$  m). The PDFs also reveal that DO achieves a maximum on each line at an intermediate  $\sigma_0$ . These parcels are at or near the surface, but have lower temperature than that of the lowest density parcels. At these lower temperatures, the water can maintain a higher DO concentration.

For each cell in the dataset we calculated the maximum oxygen concentration (OC) using solubility coefficients derived from the data of Benson and Krause (1984), as fitted by Garcia and Gordon (1992) and implemented in the gsw software package McDougall and Barker (2011). From OC, one may calculate the degree of oxygen saturation:  $\text{SO} \equiv \text{DO}/\text{OC}$  with  $\text{SO} = 1$  corresponding to a fully saturated parcel and  $\text{SO} > 1$  indicating super-saturation.

The joint PDF  $p(\theta, \text{DO})$  for  $\theta$  and DO restricted to the upper 30 m along Line 90.0 is shown in Figure 3. Overplotted on the figure is the  $\text{SO} = 1$  contour calculated at a depth of 20 m and for  $S_A = 33.7\text{gkg}^{-1}$ . There is a relatively sharp ridge in the joint PDF at  $\text{SO} \approx 1$  indicating the majority of water near the surface has approximately its maximal OC. At all temperatures, there is a tail of DO values extending beyond the  $\text{SO} = 1$  contour indicating super-saturation; these will define SO extrema as discussed below. One also notes water masses with  $T < 13\text{degC}$  and lower DO. These under-saturated parcels from a separate set of low SO extrema.

Anticipating that stratification may be influenced by oxygen super-saturation, we have calculated the buoyancy frequency  $N$  by taking the density gradient with depth  $N = (g/2\pi\rho_0)d\sigma_0/dz$ . Figure 4 shows the joint PDF for SO and  $N$ ,  $p(\text{SO}, N)$  for Line 90.0. The peak of  $p(\text{SO}, N)$  occurs at  $\text{SO} \approx 1$  and  $N = 0$ , i.e. fully saturated water with a very low buoyancy frequency. We infer this water lies within the mixed layer and is therefore in contact with the air-sea interface and air-sea fluxes maintain DO close to its maximum oxygen concentration. One also notes that the tails in the SO distribution occur preferentially at larger  $N$  values, i.e. more stratified columns.

### c. Defining Extrema in Oxygen Saturation

To examine the incidence, nature and origins of extrema in saturated oxygen near the California coast, we must first define such outliers. Figure 5 plots the cumulative distribution functions (CDFs) of SO for the top two layers ( $z = 10, 20$  m) along all four lines. It is evident from these CDFs (and Figure 4) that near the surface air-sea fluxes drive DO to its maximal OC.

However, at  $z = 10$  m approximately 80% of the water parcels exceed  $\text{SO} = 1$  and there is a tail of significantly super-saturated water. Super-saturation in the ocean may be due to the active production of DO by biological activity (e.g. phytoplankton growth) but may also indicate an out-of-equilibrium condition where the water has been recently (and rapidly) heated. On the latter point, for  $\text{SO} \approx 1$  a 1 degC increase in the water temperature yields an approximately 2% increase in SO:  $\Delta\text{SO}/\Delta T \approx 0.02(\text{degC})^{-1}$ . Our scientific interests lie in searching for signatures of enhanced SO independent of the effects related to any

<sup>1</sup>2019 for Line 56.0 when that line was added to the CUGN.

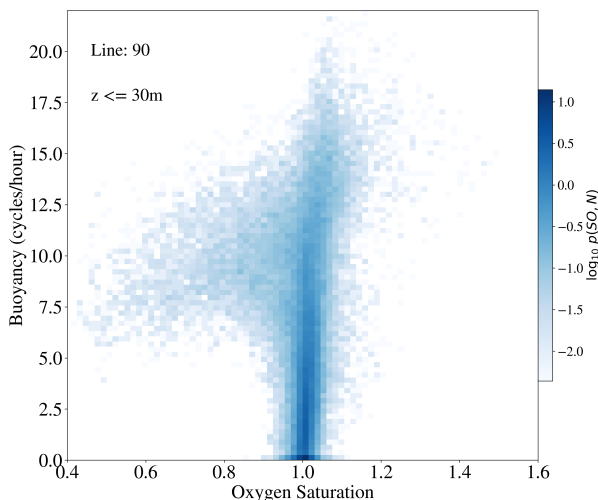


FIG. 4. Joint PDF  $p(\text{SO}, N)$  of buoyancy frequency ( $N$ ) versus oxygen saturation ( $\text{SO}$ ) for water along Line 90.0 and at depths  $z \leq 30$  m. The peak in  $p(\text{SO}, N)$  occurs at  $N = 0$  cycles  $\text{hr}^{-1}$  and  $\text{SO} = 1$ , i.e. water with fully saturated oxygen in the mixed layer. In contrast, the extrema in  $\text{SO}$ , both under-saturated and super-saturated, generally have  $N > 5$  cycles  $\text{hr}^{-1}$  which suggest a correlation between such extrema and stratification.

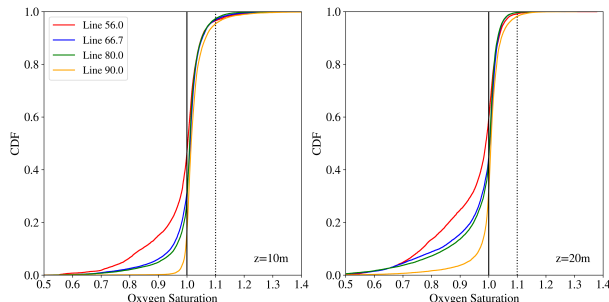


FIG. 5. Cumulative distribution functions (CDFs) of oxygen saturation  $\text{SO}$  for all water cells in the CUGN at  $z = 10$  m (left) and  $z = 20$  m (right) depth. We find  $\text{SO} \geq 1$  for the majority of cells at  $z = 10$  m and even  $\approx 50\%$  are super-saturated at  $z = 20$  m. We have defined hyperoxic extrema as  $\text{SO} \geq \text{SO}_U \equiv 1.1$  (dotted line);  $\sim 5\%$  or fewer of the parcels have such high levels along the lines. One also notes a relatively high incidence of low  $\text{SO}$ , especially along Line 56.0;  $\approx 20\%$  of its distribution shows  $\text{SO} < 0.9$  at  $z = 10$  m. We similarly construct hypoxic extrema defined as water with  $\text{SO} \leq \text{SO}_L \equiv 0.9$ .

such rapid warming<sup>2</sup>. Therefore, we define an upper extremum in  $\text{SO}$  ( $\text{SO}_U$ ) large enough to exceed changes in  $\text{SO}$  from modest temperature variations (e.g. diurnal heating). We believe a conservative choice for the CUGN is  $5\text{degC}$  corresponding to  $\text{SO}_U = 1.1$ . This temperature difference spans nearly the entire range in temperature experienced near the ocean surface throughout the analysis period (Figure 3). While our  $\text{SO}_U$  value is otherwise an arbitrary

<sup>2</sup>A small signal is expected and observed in regions with sustained warming (Emerson 1987).

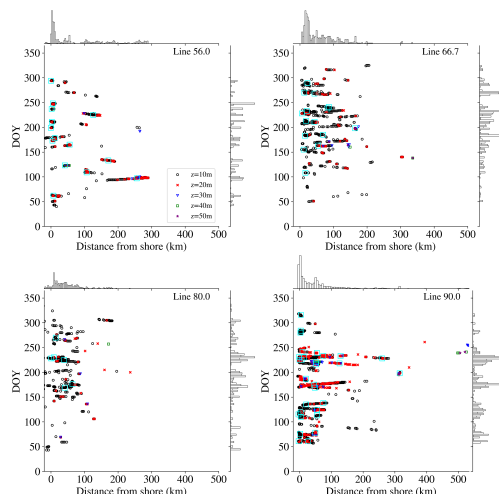


FIG. 6. Geographical (offshore distance) and temporal (day of year, DOY) distributions of the super-saturated  $\text{SO}$  extrema along each of the four lines. The water parcels satisfying  $\text{SO} > \text{SO}_U$  are marked according to their depth. On each line, the majority occur within 100 km of shore and they avoid winter months. Only Line 90.0 exhibits a high incidence of hyperoxic extrema at depths  $z > 10$  m. Overlaid on the smaller symbols are large cyan squares indicating the clustered events as defined in the text.

choice, the results presented below are largely insensitive to its choice for any value greater than 1.05.

Examining the CDF for  $\text{SO}$  (Figure 5), we find  $\text{SO} > \text{SO}_U$  for less than 5% of the water parcels along the four lines, i.e. these are truly *hyperoxic extrema*. Furthermore, the incidence of  $\text{SO} > \text{SO}_U$  is much less than 5% at  $z = 20$  m where it is less than 2% for Line 90.0 and  $< 1\%$  for the others. Other differences between Line 90 and the remainder will be emphasized in subsequent analyses.

Examining the CDFs in Figure 5 at  $\text{SO} < 1$ , one also identifies tails to  $\text{SO} < 0.7$  and below along each line at  $z = 20$  m and at  $z = 10$  m (except Line 90.0). Furthermore, we note a progression in the CDFs as one travels from south (90.0) to north (56.0) of increasing percentiles of low  $\text{SO}$ . In the following, we define *hypoxic extrema* of under-saturated water as parcels with  $\text{SO} < \text{SO}_L \equiv 0.9$ .

### 3. Results

#### a. Geographical and Temporal Distributions of $\text{SO}_U$ Extrema

Consider first the geographic and temporal signatures of super-saturated water parcels in the CUGN. Figure 6 presents the distance from shore and day of year (DOY) for hyperoxic extrema ( $\text{SO} > \text{SO}_U$ ) on all four lines of the CUGN. Geographically, on each line the majority of these extrema occur near shore, i.e. at distances less than 100 km, and primarily within 20 m of the surface. Temporally, the extrema avoid Winter months (December, January, and February), e.g. on Line 90.0, 99% occur in the interval

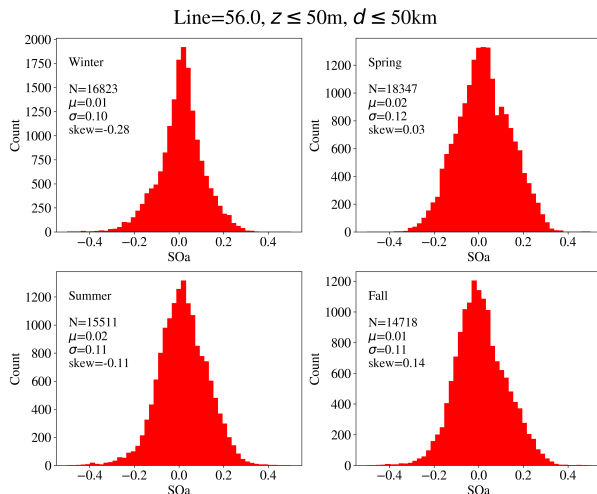


FIG. 7. Anomalies of oxygen saturation relative to the annual cycle of SO, on Line 56.0 and restricted to parcels at depth  $z \leq 50\text{m}$  and distance from shore  $d < 50\text{km}$ . The PDFs are separated by season and we provide basic statistics for each.

DOY=50–300. There is no significant differences in the seasonal distribution between the lines.

Another feature apparent in the data is that the majority are clustered in “events”, i.e. correlated in space and time. Quantitatively,  $> 90\%$  of the extrema occur within 1 day and 7 km of at least one other. With rare exceptions, the extrema are not isolated, ephemeral, or random excursions. We have generated statistically clustered events using the Density-Based Spatial Clustering of Applications with Noise (DBSCAN) algorithm (Ester et al. 1996) in the dimensions of depth, time, and distance offshore. We adopted a maximum separation of 15 days, 10 km, and 15 m in depth and required a minimum of 10 cells to define a cluster. We recover 64 clusters along the four lines, as marked in Figure 6. From this analysis, we find an average of  $\approx 2 - 5$  hyperoxic events per year on the four lines.

In a few respects, the hyperoxic extrema on Line 90 are qualitatively distinct from the others. First, this line exhibits the highest incidence of clustered events ( $\approx 5$  per year) as well as the largest such events in cells, distance, and time. Furthermore, this line exhibits a higher incidence of SO extrema below 10 m and a higher fraction within 100 km of shore. One anticipates that the conditions that generate SO extrema north of Line 90 may be physically distinct.

Lastly, none of the lines exhibit an obvious interannual trend over the 3-7 years of when DO measurements were made in the CUGN. This baseline, however, may be too short to identify any modest, interannual trend.

Figure 7 and 8 show the seasonal variations in the PDFs of anomalies of SO defined as  $SO_a \equiv SO - \overline{SO}$  with  $\overline{SO}$  the annual cycle in SO (Ren et al. 2024, submitted) us-

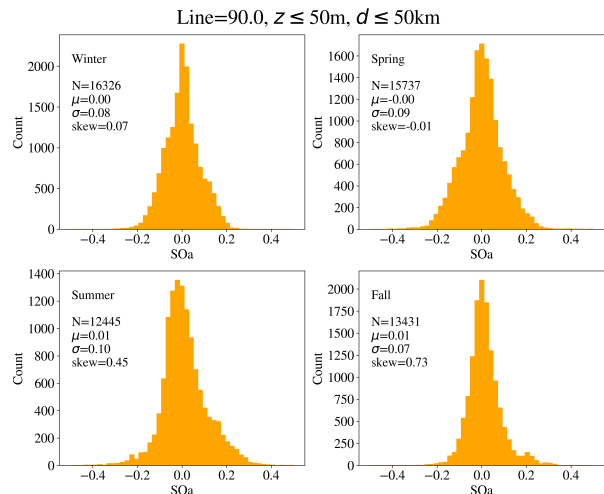


FIG. 8. Same as Figure 7 but for Line 90.0.

ing the method described in Rudnick et al. (2017). On Line 56.0, the distribution shows a significant, negative skew in the winter months indicating a higher incidence of under-saturated waters, perhaps related to upwelling activity. Later in the year, the PDFs show a small, positive skew, i.e. higher  $SO_a$  values. Contrast these results with the PDFs from Line 90.0 which never show a negative skew and which show large positive skews in the Summer and Fall months. These skews are driven by the hyperoxic extrema.

### b. Representative Examples of $SO > SO_U$ Extrema

We now examine several representative events of  $SO > SO_U$  extrema within the CUGN. Figure 9 shows the SO, DO,  $T$ , Chl  $-a$ , and  $N$  measurements for the water parcels near-shore on Line 90.0 in late-August to mid-September 2020. For this event, the majority of extrema occur subsurface at  $z \approx 20\text{m}$ . Not surprisingly the extrema show very high DO, generally at  $\approx 270 - 290 \mu\text{mol kg}^{-1}$ , and the SO values are high relative to the other parcels with  $SO < SO_U$ . Furthermore, nearly all of the extrema have an elevated buoyancy frequency of  $N > 15 \text{cycles hr}^{-1}$ . As regards temperature, the values for the extrema tend towards the median for the water probed during this 3 week interval. At both  $z = 10\text{m}$  and  $z = 20\text{m}$ , the warmest waters probed rarely satisfy the  $SO_U$  threshold, despite the fact that higher temperature means a lower, maximum oxygen concentration (i.e. higher SO for the same DO). Lastly, the Chl  $-a$  values of the extrema generally exceed  $1 \text{mg m}^{-3}$  but do not track the highest values recorded during the interval.

Figure 10 shows another near-shore event along Line 90.0, in this case during August 2021. Here, the

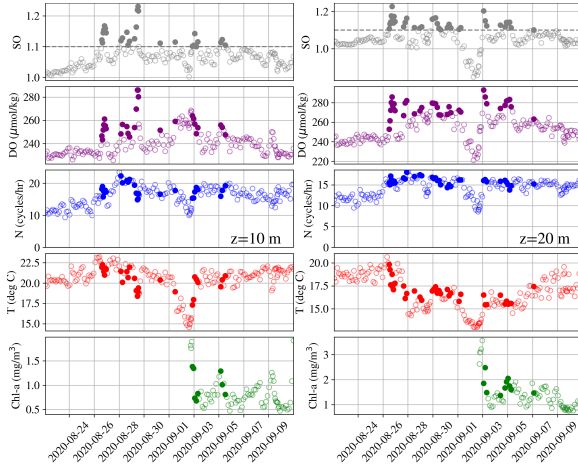


Fig. 9. SO, DO,  $N$ ,  $T$ , and Chl – a measurements for an approximately 3 week interval spanning an hyperoxic event on Line 90.0 at depth  $z = 10$  m (left) and  $z = 20$  m (right). On the first/last day of the interval, the glider is 132/86 km offshore and turns around on 2020-09-02. Filled symbols highlight the  $SO > SO_U$  extrema, which for this event are primarily at  $z = 20$  m.

extrema are primarily in the upper layer ( $z = 10$  m). The hyperoxic extrema of this event exhibit similar characteristics as for the first example: high DO values ( $> 260 \mu\text{mol kg}^{-1}$ ), elevated  $N$  ( $> 10 \text{cycles hr}^{-1}$ ), and intermediate temperature and Chl – a concentration. Also similar to the first example, the warmer waters show systematically lower DO and therefore do not satisfy  $SO > SO_U$ , although they are generally super-saturated.

Now consider a representative example (Figure 11) of an  $SO > SO_U$  event from one of the other CUGN lines. Similar to the events from Line 90.0, the super-saturated water shows very high DO values (here, primarily above  $300 \mu\text{mol kg}^{-1}$ ) and non-anomalous temperatures. In contrast to Line 90.0, however, the extrema in this event are characterized by lower buoyancy frequency and extreme Chl – a concentrations.

#### c. Representative Examples of $SO < SO_L$ Extrema

Figure 12 describes the geographic and temporal distribution of under-saturated, near-surface ( $z \leq 20$  m) waters along the four lines. The overwhelming majority of these extrema are located near-shore; except for Line 90.0,  $\approx 99\%$  lie within 100 km. In addition, the majority occur preferentially within spring or early summer (DOY=50-200).

## 4. Discussion

The previous section described the basic properties and distributions of SO extrema and examined several representative examples. We turn now to discuss plausible origins and comment on the importance of this work for studies on coastal California and the broader ocean.

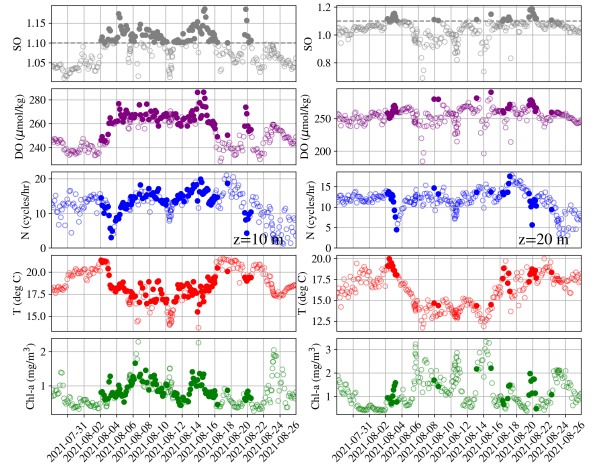


Fig. 10. As in Figure 9, a representative example of a super-saturated event along Line 90.0 but now primarily within the upper,  $z = 10$  m layer. We otherwise find the hyperoxic extrema have similar characteristics (high DO, high  $N$  and intermediate temperature and Chl – a).

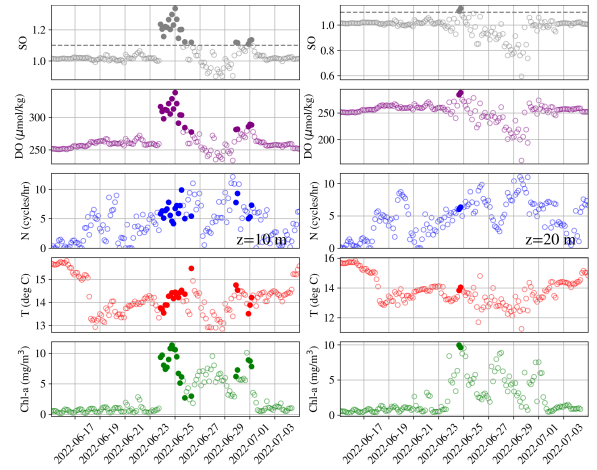


Fig. 11. Example of a hyperoxic event along Line 80.0. In contrast to the examples from Line 90.0, the events along the other lines tend to have shorter duration, lower  $N$  values, and much higher Chl – a concentration.

#### a. The Principal Drivers of Hyperoxic Extrema along Coastal California

In the CUGN, hyperoxic events occur most frequently within 100 km of shore, within 30 m of the ocean surface, and in non-winter months. They frequently occur in events lasting several days to several weeks.

As we explore the primary drivers of such extrema, we remind the reader that for the DO in a given water parcel to (at least temporarily) exceed its maximum oxygen concentration, either the OC has been lowered by increasing the temperature (without lowering DO) and/or biological productivity has increased DO within the water. In the representative examples along Line 90.0 (Figures 9,

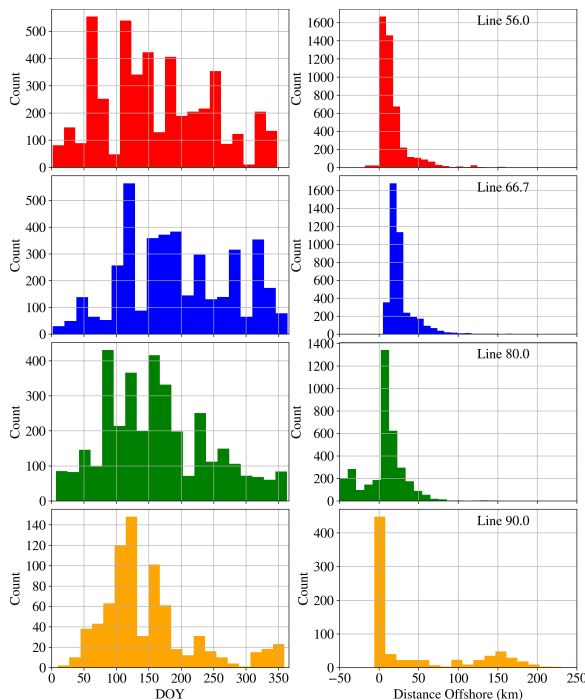


FIG. 12. Temporal (DOY, left) and geographical (distance from shore, right) distributions of the hypoxic extrema ( $SO < SO_L$ ) near the surface ( $z \leq 20$  m) along the four lines. These extrema are located primarily near shore, in regions most affected by upwelling. For Lines 80.0, 90.0, they also occur most frequently in spring and early summer.

10), there is no signature of elevated temperature in the hyperoxic extrema. In fact, if anything the  $SO > SO_U$  extrema show cooler temperatures than their surrounding waters. To further examine the potential role of temperature, for Line 90.0 we have calculated the temperature anomaly of the extrema relative to the annual cycle calculated by (Rudnick et al. 2017). Figure 13 compares these with all parcels on Line 90.0 restricted to  $z \leq 20$  m. The distributions of both the hyperoxic extrema and the control sample peak at 0 deg C with a symmetric distribution spanning  $\approx \pm 2$  deg C. There is no systematic trend of the  $SO > SO_U$  extrema towards unusually warm temperatures, and nothing approaching the  $\approx 5$  deg C that would be required to bring marginally saturated water to  $SO > 1.1$ . We conclude, therefore, that the primary driver of extreme super-saturated water is not a rapid rise in temperature.

This requires, therefore, that the extrema originate from an elevated DO concentration. Indeed, when examining the representative examples we stressed the presence of high DO values both in absolute terms and relative to nearby water parcels not satisfying the  $SO_U$  threshold. We test this inference statistically by comparing the DO distribution of the  $SO > SO_U$  extrema along each line to that from a custom control sample. For the latter, we used the joint PDF grid of absolute salinity and potential density shown in Figure 1

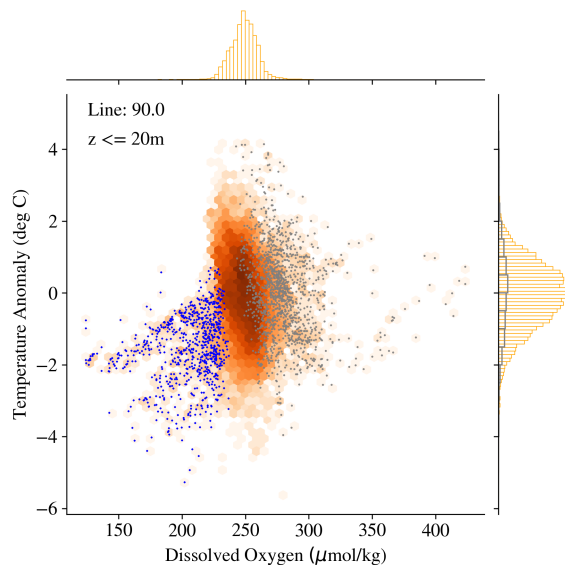


FIG. 13. Joint distribution of temperature anomalies measured relative to the annual cycle versus dissolved oxygen restricted to Line 90.0 and  $z \leq 20$  m. Overplotted as dots on the joint PDF are the hyperoxic (gray) and hypoxic extrema (blue). The former are distributed uniformly in temperature (compare the histograms) whereas the hypoxic extrema occur almost exclusively at colder than average temperature.

restricted to those cells with at least 50 samples. For every hyperoxic extremum, we take at random 5 parcels in the same  $S_A, \sigma_\theta$  bin and the ensemble is the matched control sample.

Figure 14 shows the CDFs of the DO distributions for the extrema versus that of the control sample. Clearly, the DO distribution of the extrema well exceed that of the control sample confirming a systematic DO excess. We now consider conditions that may drive this excess.

In addition to elevated DO, the representative hyperoxic events along Line 90.0 also the hyperoxic parcels show a high buoyancy frequency (frequently  $N > 15$  cycles  $hr^{-1}$ ). This suggests that stratification may be a physical factor driving higher DO along Line 90.0. To explore this hypothesis further, Figure 15 compares the CDFs of  $N$  for all  $SO > SO_U$  parcels against the same control sample as described above for DO. The results for Line 90.0 confirm that high buoyancy frequency is a predominant trait of hyperoxic water near the coast of San Diego. Physically, stratification serves to isolate these waters from the surface to prevent air-sea fluxes from driving DO down to the maximum allowed oxygen concentration given its temperature (i.e.  $SO \approx 1$ ).

We also recall from Figures 9 and 10, however, that a majority of the water exhibits  $N > 10$  cycles  $hr^{-1}$  during those events, including parcels with  $SO < SO_U$  (although still saturated). The implication is that stratification is a necessary, albeit insufficient property to achieve the highest

saturation levels. We further recall in these events that the  $\text{Chl} - a$  concentration, which often indicates enhanced productivity, does not exhibit the highest values of the event. The values do generally exceed  $0.2 \text{ mg m}^{-3}$  but are not extrema. This point is statistically emphasized in Figure 16 which shows the CDFs of  $\text{Chl} - a$  for hyperoxic extrema on Line 90.0 are nearly consistent with the control sample. We hypothesize an additional factor not captured by sensors on the CUGN gliders – perhaps enhanced nutrient content from recent upwelling – is at work.

Consider next Line 56.0, the northernmost part of the CUGN. Referring to Figures 15, we find the buoyancy frequency CDF for the SO extrema is consistent with the control sample. We therefore conclude that stratification is not a primary factor and further note that nearly all of the extrema occur at the shallowest depth, i.e. in or just below the mixed layer. On the other hand, the  $\text{Chl} - a$  CDF for Line 56.0 is greatly skewed to higher concentrations (Figure 16). For hyperoxic water to occur on this line, an intense bloom of productivity may be required. In contrast with Line 90.0, we hypothesize the weaker stratification implies a higher flux at the air-sea interface which drives the oxygen saturation to 100% unless the DO generation greatly exceeds this flux.

Turning to the other Lines, these tend towards lower buoyancy frequencies than Line 90.0 (but still elevated). This is well described by the CDFs in Figure 15. Furthermore, as one travels North along the California coast, the  $\text{Chl} - a$  concentration of the extrema increases, both in absolute terms and relative to the control sample (Figure 16). In essence, the characteristics of the hyperoxic extrema on Lines 66.7 and 80 lie intermediate to the extrema on Lines 56.0 and 90.0. We expect, therefore, that their hyperoxic events are due to milder blooms in more stratified (i.e. less ventilated) waters.

### b. Origin of Hypoxic Extrema

We comment briefly on the origin(s) of the near-surface, hypoxic extrema in the CUGN. Figure 12 shows that these are preferentially within 100 km of shore for Lines 56.0, 67.5, and 80.0 and at both  $< 100 \text{ km}$  and  $\approx 150 \text{ km}$  on Line 90.0. These geographic regions are the primary locations of upwelling along each line, including the secondary peak at  $\approx 150 \text{ km}$  on Line 90.0 due to the Santa Rosa Ridge. Furthermore, except for Line 56.0, the majority of these extrema occur during spring or early summer (DOY=50-200) which are the most common times for the wind-driven upwelling of the CUGN system.

We note further that these extrema have temperatures lower than the annual mean at their location and depth (Figure 13). This is yet another indication that upwelling drives these events. In addition, the trend towards a higher incidence of under-saturated SO as one travels north (Figure 5) is consistent with the hypothesis. Last, the modest but

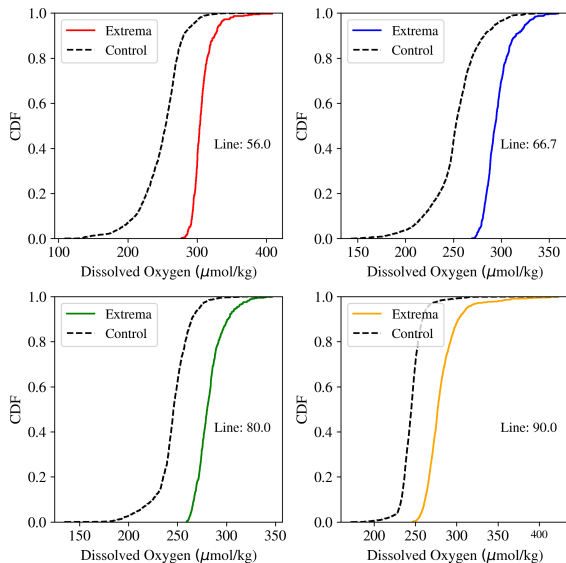


FIG. 14. Cumulative distribution functions (CDFs) for dissolved oxygen for the  $\text{SO} > \text{SO}_U$  extrema (solid lines) along each CUGN line. For each line, we have generated a control sample matched to the extrema in absolute salinity and potential density and restricted to depths  $z \leq 50 \text{ m}$ . The CDFs of the extrema show systematically higher DO values, as expected.

non-zero buoyancy frequency values ( $N \approx 5 \text{ cycles hr}^{-1}$ ; Figure 4) imply the water has not mixed fully with the surface. We conclude that the near-surface, under-saturated waters in the CUGN arise primarily from low-DO waters during upwelling episodes.

### c. Previous Studies in the California Current System

Previous studies on extrema of dissolved oxygen in the California current system have focused on hypoxic events (e.g. Grantham et al. 2004; Chan et al. 2008). The most extreme of these have had significantly negative impacts on the ecosystem. The dominant driver of these episodes is believed to be the advection of abnormally low dissolved oxygen into the system in combination with the upwelling of nutrient-rich but oxygen-depleted water. Furthermore, hypoxia in the upper waters during these events may be linked to sustained stratification that prevents or reduces ventilation Bograd et al. (2008). Ironically, we have found stratification can play the same role (reduced ventilation) but with the opposite outcome – hyperoxic events along Line 90.0. An accurate estimate of the physical state of the California Current system, therefore, is central to predicting biological processes.

## 5. Conclusions

This study has characterized the extremes of dissolved oxygen saturation in the California Current System using



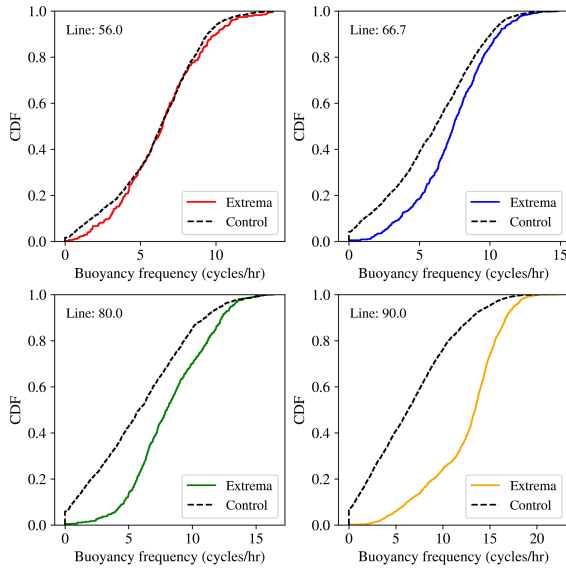


Fig. 15. Similar to Figure 14 but for buoyancy frequency. For these results, the extrema show increasingly higher  $N$  values and larger offsets from the control sample as one travels from north (Line 56.0) to south (Line 90.0) down the California coast.

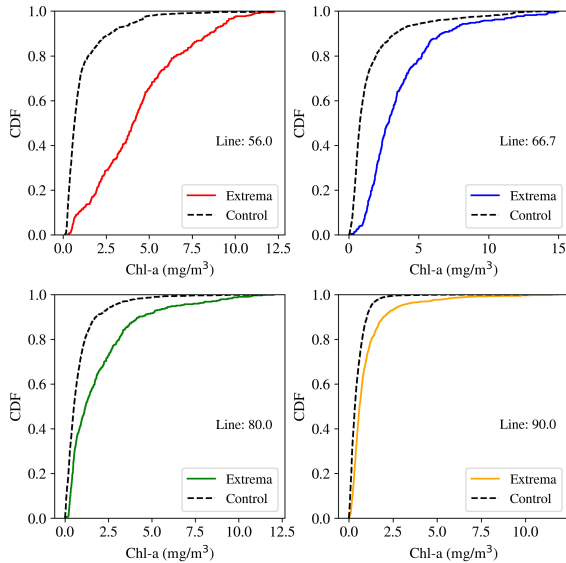


Fig. 16. Similar to Figure 14 but for Chl – a concentration. Opposite to the results to for buoyancy frequency, we find the extrema nearly match the control sample along Line 90.0 and show higher concentrations and greater offset as one travels from south to north along the coast.

data from the California Underwater Glider Network. Hypoxic events, defined as water parcels with oxygen saturation exceeding 110%, were found to occur primarily within 100 km of shore, in the upper 30 m of the water column, and during non-winter months. The drivers of these events appear to vary along the coast. Along Line 90.0 near San

Diego, hyperoxic extrema are associated with high stratification, which may isolate sub-surface waters and allow biological production to elevate dissolved oxygen levels above saturation. In contrast, along the northernmost Line 56.0, hyperoxic events occur primarily at the surface and are strongly correlated with elevated chlorophyll-a concentrations, suggesting they are driven by intense phytoplankton blooms. Lines 66.7 and 80.0 show intermediate characteristics, with hyperoxic events likely resulting from moderate blooms in somewhat stratified waters.

Hypoxic extrema, defined as near-surface waters with oxygen saturation below 90%, were found to occur predominantly within 100 km of shore and during spring or early summer. These events are consistent with coastal upwelling bringing low-oxygen waters to the surface. The incidence of these hypoxic events increases from south to north along the California coast, reflecting the stronger influence of upwelling in the northern part of the study region. These findings highlight the complex interplay between physical processes like stratification and upwelling, and biological processes such as primary production, in shaping the dissolved oxygen dynamics of the California Current System. Understanding these extremes and their drivers is crucial for predicting ecosystem responses to changing ocean conditions and for improving biogeochemical models of this important coastal system.

*Acknowledgments.* J.X.P. and D.L.R. acknowledge support by the Simons Foundation.

*Data availability statement.* All of the data analyzed within are available as products of the CUGN Rudnick (2016). All of the code used to perform analysis is available on GitHub (Prochaska 2024).

## References

- Benson, B. B., and J. Krause, Daniel, 1984: The concentration and isotopic fractionation of oxygen dissolved in freshwater and seawater in equilibrium with the atmosphere. *Limnology and Oceanography*, **29** (3), 620–632, <https://doi.org/10.4319/lo.1984.29.3.0620>.
- Bograd, S. J., C. G. Castro, E. Di Lorenzo, D. M. Palacios, H. Bailey, W. Gilly, and F. P. Chavez, 2008: Oxygen declines and the shoaling of the hypoxic boundary in the California Current. *Geophysical Research Letters*, **35** (12), L12607, <https://doi.org/10.1029/2008GL034185>.
- Bopp, L., and Coauthors, 2013: Multiple stressors of ocean ecosystems in the 21st century: projections with CMIP5 models. *Biogeosciences*, **10** (10), 6225–6245, <https://doi.org/10.5194/bg-10-6225-2013>.
- Chan, F., J. A. Barth, J. Lubchenco, A. Kirincich, H. Weeks, W. T. Peterson, and B. A. Menge, 2008: Emergence of Anoxia in the California Current Large Marine Ecosystem. *Science*, **319** (5865), 920, <https://doi.org/10.1126/science.1149016>.
- Emerson, S., 1987: Seasonal oxygen cycles and biological new production in surface waters of the subarctic Pacific Ocean. *Journal of Geophysical Research*, **92** (C6), 6535–6544, <https://doi.org/10.1029/JC092iC06p06535>.
- Ester, M., H.-P. Kriegel, J. Sander, and X. Xu, 1996: A Density-Based Algorithm for Discovering Clusters in Large Spatial Databases with Noise. *Second International Conference on Knowledge Discovery and Data Mining (KDD'96). Proceedings of a conference held August 2-4*, 226–331.
- Fennel, K., J. Wilkin, J. Levin, J. Moisan, J. O'Reilly, and D. Haidvogel, 2006: Nitrogen cycling in the middle atlantic bight: Results from a three-dimensional model and implications for the north atlantic nitrogen budget. *Global Biogeochemical Cycles*, **20** (3), <https://doi.org/https://doi.org/10.1029/2005GB002456>, <https://agupubs.onlinelibrary.wiley.com/doi/pdf/10.1029/2005GB002456>.
- Garcia, H. E., and L. I. Gordon, 1992: Oxygen solubility in seawater: Better fitting equations. *Limnology and Oceanography*, **37** (6), 1307–1312, <https://doi.org/10.4319/lo.1992.37.6.1307>.
- Giomi, F., and Coauthors, 2019: Oxygen supersaturation protects coastal marine fauna from ocean warming. *Science Advances*, **5** (9), eaax1814, <https://doi.org/10.1126/sciadv.aax1814>.
- Grantham, B. A., F. Chan, K. J. Nielsen, D. S. Fox, J. A. Barth, A. Huyer, J. Lubchenco, and B. A. Menge, 2004: Upwelling-driven nearshore hypoxia signals ecosystem and oceanographic changes in the northeast Pacific. *Nature*, **429** (6993), 749–754, <https://doi.org/10.1038/nature02605>.
- Helm, K. P., N. L. Bindoff, and J. A. Church, 2011: Observed decreases in oxygen content of the global ocean. *Geophysical Research Letters*, **38** (23), L23602, <https://doi.org/10.1029/2011GL049513>.
- IOC, SCOR and IAPSO, 2010: The international thermodynamic equation of seawater – 2010: Calculation and use of thermodynamic properties. Manuals and Guides 56, Intergovernmental Oceanographic Commission, 196 pp. <https://doi.org/10.25607/OBP-1338>, URL <http://dx.doi.org/10.25607/OBP-1338>.
- Keeling, R. F., and H. E. Garcia, 2002: The change in oceanic O<sub>2</sub> inventory associated with recent global warming. *Proceedings of the National Academy of Science*, **99** (12), 7848–7853, <https://doi.org/10.1073/pnas.122154899>.
- McDougall, T. J., and P. M. Barker, 2011: *Getting started with TEOS-10 and the Gibbs Seawater (GSW) Oceanographic Toolbox*. SCOR/IAPSO WG127, 28 pp.
- Prochaska, J. X., 2024: AI-for-Ocean-Science/cugn: Release with the paper submission on Saturated Oxygen. Zenodo, <https://doi.org/10.5281/zenodo.13333073>, <https://doi.org/10.5281/zenodo.13333073>.
- Ren, A. S., D. L. Rudnick, and A. Twombly, 2023: Drift Characteristics of Sea-Bird Dissolved Oxygen Optode Sensors. *Journal of Atmospheric and Oceanic Technology*, **40** (12), 1645–1656, <https://doi.org/10.1175/JTECH-D-22-0103.1>.
- Rudnick, D., 2016: California underwater glider network. <https://doi.org/10.21238/S8SPRAY1618>.
- Rudnick, D. L., K. D. Zaba, R. E. Todd, and R. E. Davis, 2017: A climatology of the California Current System from a network of underwater gliders. *Progress in Oceanography*, **154**, 64–106, <https://doi.org/10.1016/j.pocean.2017.03.002>.
- Schmidtko, S., L. Stramma, and M. Visbeck, 2017: Decline in global oceanic oxygen content during the past five decades. *Nature*, **542** (7641), 335–339, <https://doi.org/10.1038/nature21399>.